Desalination and Water Treatment
www.deswater.com

doi: 10.5004/dwt.2017.20742

96 (2017) 12–21
November

Polyvinylidene fluoride membranes with enhanced antibacterial and low fouling properties by incorporating ZnO/rGO composites

Woon Chan Chong[a,b], Ebrahim Mahmoudi[a], Ying Tao Chung[a,c], Muneer M. Ba-Abbad[a,d], Chai Hoon Koo[e], Abdul Wahab Mohammad[a,b,*]

[a]*Department of Chemical and Process Engineering, Faculty of Engineering and Built Environment, Universiti Kebangsaan Malaysia, 43600 Bangi, Selangor, Malaysia, emails: drawm@ukm.edu.my (A.W. Mohammad), chongwoonchan@gmail.com (W.C. Chong), ebi.dream@gmail.com (E. Mahmoudi), cytao518@gmail.com (Y.T. Chung), muneer711@gmail.com (M.M. Ba-Abbad)*
[b]*Department of Chemical Engineering, Lee Kong Chian Faculty of Engineering and Science, Universiti Tunku Abdul Rahman, Jalan Sungai Long, Bandar Sungai Long, Cheras, 43000 Kajang, Selangor, Malaysia*
[c]*Fuel Cell Institute, Universiti Kebangsaan Malaysia, 43600 Bangi, Selangor, Malaysia*
[d]*Research Center for Sustainable Process Technology (CESPRO), Faculty of Engineering and Built Environment, Universiti Kebangsaan Malaysia, 43600 Bangi, Selangor, Malaysia*
[e]*Department of Civil Engineering, Lee Kong Chian Faculty of Engineering and Science, Universiti Tunku Abdul Rahman, Jalan Sungai Long, Bandar Sungai Long, Cheras, 43000 Kajang, Selangor, Malaysia, email: kooch@utar.edu.my*

Received 26 January 2017; Accepted 20 March 2017

ABSTRACT

In this study, the performance enhancement of polyvinylidene fluoride (PVDF) polymer as one of the most hydrophobic membrane material, blended with zinc oxide (ZnO) and zinc oxide/reduced graphene oxide (ZnO/rGO) was investigated. ZnO/rGO composites which acted as inorganic filler were synthesized via a facile precipitation method using zinc nitrate ($Zn(NO_3)_2$) as zinc precursor and sodium hydroxide (NaOH) as reducing agent. The synthesized ZnO/rGO composites with various Zn loadings were analyzed in terms of particles size and surface charge. The composites with highest surface charge and smallest particles size were then selected for PVDF membrane fabrication. The membranes were produced via immersion-precipitation method and they were characterized by water permeation test, contact angle, morphology, bovine serum albumin (BSA) rejection, flux recovery and antibacterial activity. Based on the findings, ZnO/rGO composites gave the most hydrophilic effect to the PVDF membranes, resulted in 61% of permeation flux increment in comparison with neat PVDF membranes. Simultaneously, the ZnO/rGO mixed matrix membranes (MMMs) showed the highest BSA rejection of 32% and flux recovery ratio of 48%, implying the improvement of the membranes' fouling resistance. Besides, there was no release of Zn element in permeate of ZnO/rGO MMMs which implied the strong bonding between ZnO/rGO composite with PVDF membranes. In addition, the superior antibacterial property of ZnO/rGO MMMs showed great potential in biofouling mitigation. Hence, the utilization of ZnO/rGO MMMs was highly recommended in various applications involving fouling and biofouling issues.

Keywords: ZnO; Graphene oxide; Antibacterial; Biofouling; Mixed matrix membranes

* Corresponding author.

Presented at the 9th International Conference on Challenges in Environmental Science & Engineering (CESE-2016), 6–10 November 2016, Kaohsiung, Taiwan.

1. Introduction

The demand of ultrafiltration (UF) membrane in water and wastewater treatment application has increased significantly in recent years. Countries in Asia Pacific and Middle East regions such as Malaysia, Australia, Qatar and Saudi Arabia emerged as the key drivers in the UF membrane market due to water stress issue and increasing environmental awareness [1]. The UF membrane technology is favorable as it produces high quality effluent with relatively low operating pressure in reclamation and recycling of municipal, agriculture and industrial wastewater sector [2]. However, to date, membrane fouling still remains one of the crucial issues to be addressed in developing a more sustainable membrane filtration system.

Continuous research has been carried out in mitigating membrane fouling issue. Modifying surface properties of membrane by blending with hydrophilic nanoparticles in membrane fabrication process is one of the promising ways to increase permeation flux while mitigating membrane fouling propensity [3,4]. Previous studies have shown that incorporation of nanoparticles such as titanium oxide (TiO_2) [5,6], silver (Ag) [7,8], zinc oxide (ZnO) [9,10] and aluminum oxide (Al_2O_3) [11] into various polymeric membranes had successfully improved permeation flux and rejection performance of the membranes. Among the nanoparticles, ZnO is getting greater attention in water treatment research due to its lower synthesis cost, great photocatalytic activity under natural sunlight and good antibacterial property [12,13]. Studies have shown that membrane surface charge [14], particle size distribution [12,13] and concentration of fillers [15] are significant factors in determining mixed matrix membranes (MMMs) structure, filtration performance and extent of membrane fouling.

The benefits of zeta potential study of particles utilization in the industry had been emphasized by Marsalek [16]. Membrane with highly negative surface charge would be able to repel flocs which are negatively charged in nature. Besides, smaller size nanoparticles with high area-to-volume ratio are able to increase the hydrophilicity of membrane. In a study done by Leo et al. [15], the addition of 2 wt% of ZnO in polysulfone (PSF) polymer had successfully reduced the membrane contact angle from 85° to 62°, and significantly improved the performance of the MMMs. However, higher amount of ZnO nanoparticles incorporated in polymeric membrane would result in decrement of permeation flux due to agglomeration of ZnO nanoparticles inside the membranes, hindering the formation of bigger pores [14,15]. To improve the stability of ZnO nanoparticles over agglomeration, the nanoparticles were coated with various capping agents such as sodium dodecyl sulfate, cetyltrimethylammonium bromide [17] and polyvinylpyrrolidone (PVP) [18] which provide steric forces to keep the nanoparticles separated from each other. In a membrane study by Chung et al. [13], the addition of ethylene glycol functionalized ZnO nanoparticles in PSF polymer had reduced ZnO nanoparticles size and prevented agglomeration, hence enhancing the membrane performance in terms of permeation flux, thermal stability and humic acid rejection.

Recently, functionalization of metal oxide on graphene oxide (GO) shows promising outcome in increasing the membrane hydrophilicity [6,7]. The abundance of oxygen functional groups (epoxy and hydroxyl) in GO could act as nucleation sites for the growth of metal oxide. Hence, metal oxide could distribute evenly on GO and the overall effective surface area of metal oxide could be enhanced [6,19]. Furthermore, GO is an excellent inorganic filler in various polymeric membranes due to its high hydrophilicity and negative surface charge [20,21]. The effect of ZnO impregnated GO incorporated in the polyvinylidene fluoride (PVDF) membranes was first investigated in this study. The ZnO/rGO composites were expected to add values on the PVDF membranes by increasing its hydrophilicity with enhanced antibacterial property. The neat PVDF membranes, ZnO MMMs and ZnO/rGO MMMs were characterized and evaluated in terms of permeability, hydrophilicity, morphology, leaching and antibacterial property. Besides, bovine serum albumin (BSA) as model protein (major foulant in biological wastewater) was used to evaluate the rejection and antifouling ability of the membranes.

2. Experimental setup

2.1. Material

GO was synthesized using modified Hummers' method [7]. Other chemicals used for synthesis of ZnO/rGO composites were zinc nitrate ($Zn(NO_3)_2$, 98%, VWR, England), sodium hydroxide (NaOH) and PVP, used as received without further purification.

The PVDF membranes were made from Solef 6010 (Solvay, Belgium), purchased in powder form. *N*,*N*-Dimethylacetamide (DMAc, ≥99.5%, Sigma-Aldrich, Germany) was used as solvent to dissolve the polymer. BSA (Nacalai Tesque, Japan) was used to prepare feed solution for membrane fouling performance test. Zinc oxide (ZnO, Sigma-Aldrich, Germany) nanoparticles with average particle size <100 nm and self-synthesized ZnO/rGO composites were used as fillers for the membranes. Pure water used for membrane filtration in this study was from Sartorius arium pro ultrapure water system.

2.2. Synthesis of ZnO/rGO composites

Initially, 0.2 g GO powder was dispersed into 100 mL absolute ethanol (99%) and stirred rigorously to achieve homogenous condition followed by sonication for 30 min. Different amount of $Zn(NO_3)_2$ (10, 30, 60 and 100 wt% of Zn with respect to the amount of GO) with PVP was dissolved and added slowly into the GO solution with rigorous stirring for 1 h. Next, 0.20 M of NaOH as the reducing agent was added slowly into the mixture of GO solution and stirred continuously for 3 h. The precipitate formed was then sonicated for 15 min, washed with centrifugation for at least two times with deionized water before drying, followed by calcination at 400°C under continuous flow of nitrogen gas.

2.3. ZnO/rGO composites characterization

The crystallite size and crystal phase composition of synthesized ZnO attached on GO were studied using a X-ray diffractometer (XRD) with Cu Kα radiation (1.5406 Å) for a

scan range of 20°–80° in a 2 h scan (Bruker, D8 Advance AXS XRD). Subsequently, the average crystallite size of the ZnO was determined using the Debye–Scherrer equation.

The zeta potential of the composites and membranes were determined using Zetasizer (Malvern, Nano ZS). The composites in powder form were dispersed into water and sonicated for 20 min before the analysis. Zeta potential of ZnO powder was measured as a comparison with the ZnO/rGO composites.

The morphology and distribution of ZnO on GO were observed via ultrahigh resolution field-emission scanning electron microscope (UHR-FESEM; Zeiss, Germany; MERLIN) with energy dispersive X-ray spectrometer (EDX) and transmission electron microscopy (TEM; Zeiss, Germany; Libra-120). For TEM sample preparation, sample powder were prepared by placing a drop of powder solution (ethanol as solvent) onto a carbon-coated copper grid with 300 mesh followed by drying in air before analysis.

2.4. Membrane fabrication

The casting solutions were prepared by dissolving 18 wt% of PVDF powder into DMAc solvent. Upon complete dissolution of PVDF powder, 0.4 wt% of ZnO nanoparticles or ZnO/rGO composites were added into the casting solutions and stirred continuously for 3 h to form homogeneous solutions. After that, the casting solutions were sonicated for 1 h to remove the bubbles and left overnight for degas. The membranes were casted on polyester non-woven fabric with thickness of 0.2 mm using filmographe doctor blade (Braive Instrument, Germany). Subsequently, the membranes were immersed into coagulation bath in room temperature. The membranes formed were immersed in water for 24 h for completed phase inversion.

2.5. Membrane characterization

The Fourier transform infrared (FTIR) spectra of the membranes were obtained using FTIR spectrometer (Thermo Scientific, USA; NICOLET 6700), ranging from 350 to 4,000 cm^{-1}.

The hydrophilicity of neat PVDF membranes and MMMs were determined with sessile-drop method by using contact angle meter (Kruss GmbH, Germany).

Atomic force microscopy (AFM) studies were conducted to investigate the effect of ZnO and ZnO/rGO on membrane surface roughness by the means of scanning probe microscopy (NT-MDT, NTEGRA Prima). Roughness parameters were analyzed using Image Analysis P9 (NT-MDT) software. The membrane surface and sectional structure were observed using UHR-FESEM (Zeiss, MERLIN). EDX was used to confirm the presence of Zn element in the MMMs.

The membrane porosity, ε was determined using gravimetric method as shown in Eq. (1):

$$\varepsilon = \frac{W_1 - W_2}{Al\rho_w} \times 100\% \tag{1}$$

where W_1 (kg) is weight of wet membrane, W_2 (kg) is weight of dried membrane, A (m^2) is membrane area, l (m) is membrane thickness and ρ_w (kg/m^3) is water density. Meanwhile, pore size formed in the membranes, r_m was estimated using Guerout–Elford–Ferry equation as shown in Eq. (2):

$$r_m = \sqrt{\frac{(2.9 - 1.75\varepsilon)8\eta l Q}{\varepsilon A \Delta P}} \tag{2}$$

where η (Pa s) is viscosity of water, Q (m^3/s) is volume of pure water collected as permeate and ΔP (Pa) is operational pressure.

Filtration experiment was further performed to measure the release of zinc from MMMs. Pure water was filtered through the ZnO MMMs and ZnO/rGO MMMs at 2 bar for 6 h. The permeate samples were analyzed by inductively coupled plasma optical emission spectrometry (PerkinElmer, Turkey; Optima 7000).

2.6. Membrane performance test

For pure water permeation test, each membrane was pressurized for 30 min at 3 bar using pure water. After that, all filtration experiments were carried out at 2 bar using a stirred cell. Permeation flux was calculated with Eq. (3):

$$J = \frac{V}{At} \tag{3}$$

where J (L/m^2 h) is permeation flux, V (L) is volume of permeate collected, A (m^2) is membrane area and t (h) is time taken for filtration.

Membrane filtration was continued by replacing pure water with 1,000 ppm BSA solution in the same filtration condition. BSA rejection, R was calculated using Eq. (4):

$$R = \frac{C_1 - C_0}{C_0} \times 100\% \tag{4}$$

where C_0 and C_1 are initial and final concentration of BSA, respectively, in ppm.

Besides, permeation flux of BSA filtration was recorded for 150 min for all the membranes. Subsequently, the membranes were cleaned with pure water and BSA feed solution was replaced with pure water again. The pure water flux was remeasured in order to get flux recovery ratio (FRR) as shown in Eq. (5):

$$\text{FRR} = \frac{J_{w_2}}{J_{w_1}} \times 100\% \tag{5}$$

where J_{w_1} (L/m^2 h) is initial permeation flux of pure water and J_{w_2} (L/m^2 h) is permeation of pure water after BSA filtration.

2.7. Antibacterial test

In this study, *Escherichia coli* (Gram negative) was chosen as a model biofoulant for the antibacterial test. Previous

studies had proven that *E. coli* has higher resistance to ZnO compared with *Staphylococcus aureus* (Gram positive) due to difference of membrane cell polarity [22,23]. The higher negative charge of *E. coli* hindered penetration of hydrogen peroxide (a type of reactive oxygen species [ROS] generated by ZnO) into the bacterial cell and subsequently destroyed the cellular components. Therefore, only *E. coli* was tested in this study. First, the membranes were placed on nutrient agar plates. Then, 10 μL of nutrient with *E. coli* (20×10^7 CFU/mL) was dropped on each membrane. Subsequently, they were incubated overnight at 37°C. The growth of *E. coli* on membrane surface were observed using UHR-FESEM.

3. Results and discussion

3.1. ZnO/rGO composites characterization

3.1.1. Effect of ZnO loadings on physical properties of ZnO/rGO composites

Fig. 1 presents the XRD patterns of ZnO/rGO composites with various $Zn(NO_3)_2$ concentration. The peaks as shown in 2θ values of 31.68°, 34.27°, 36.07°, 47.35°, 56.8°, 62.72°, 67.13°, 67.83° and 68.95° corresponded to the Miller index of the reflecting planes for (100), (002), (101), (102), (110), (103), (200), (112) and (201) (JCPDS card no. 36-1451). All the ZnO formed are in polycrystalline nature with hexagonal wurtzite structure. The disappearance of prominent peak of GO around 10.89° was unavoidable due to thermal reduction during heat treatment where formation and desorption of water molecules from GO occurred [24]. Therefore, the GO was partially reduced.

Referring to the XRD data in Fig. 1, the calculated crystallite size of ZnO attached on GO nanosheets for 10, 30, 60 and 100 wt% of Zn were 11.68, 12.42, 13.31 and 16.34 nm, respectively. The result showed that crystallite size grew with the increasing of zinc precursor concentration. This was in agreement with the observations reported by Zhao et al. [25] and Malek et al. [26], where the nucleation and growth rates of ZnO were relatively slow for lower concentration of zinc. When the concentration of zinc increased, the supersaturation condition increased and therefore increasing the nucleation rate [27]. Furthermore, when the GO nanosheets covered with high amount of ZnO, smaller size of ZnO crystals would coalesce into larger particles via oriented attachment mechanism where their side crystal planes would stick

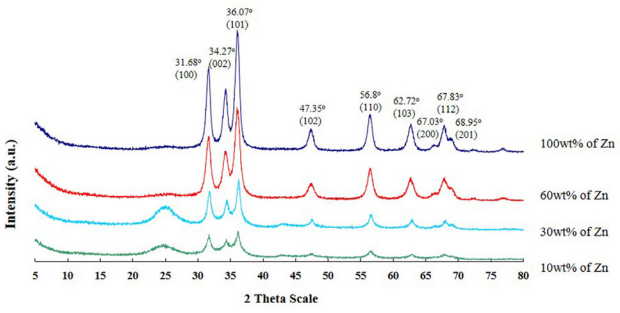

Fig. 1. X-ray diffraction (XRD) patterns of ZnO/rGO composites for various loading of Zn.

to each other [25]. This was further proven by UHR-FESEM findings in section 3.1.2 where higher concentration of zinc precursor would lead to formation of larger size of ZnO and tend to form plane structure.

Besides, the surface charge of ZnO/rGO composites with various amount of Zn was measured at pH 7. The zeta potential of pure ZnO was +9.98 mV, meanwhile the zeta potential of ZnO/rGO composites for 10, 30, 60 and 100 wt% of Zn were –26.97, –17.13, –10.4 and –7.45 mV, respectively. The zeta potential negativity of ZnO/rGO composites was found to decrease with the increase of ZnO content. This could be explained by the dominance of ZnO surface charge when the GO surface area was covered by higher amount of ZnO. GO nanosheets which served as a decoration platform for ZnO had successfully tuned the surface charge of these nanohybrids from positive to negative. Surface charge did play a significant role in foulant rejection in UF. A high negatively charged membrane would be able to repel foulant which are normally negatively charge in nature and hence increase the overall rejection during filtration process [28].

3.1.2. Particle distribution of ZnO on GO nanosheets

The surface morphology and distribution of ZnO in the composites were characterized by UHR-FESEM and depicted in Fig. 2 at magnification of 30,000× and 100,000×. At high Zn concentration, the small particle of ZnO prone to embed with each other and form larger particle size [25,26]. As shown in Figs. 2(a) and (b), the GO nanosheets were highly decorated with ZnO nanoparticles, resulting in the particles sticking together and formed flakes. On the other hand, the size of ZnO nanoparticles formed with 60 wt% (Figs. 2(c) and (d)) and 30 wt% of Zn (Figs. 2(e) and (f)) were found relatively large and scattered on the surface of GO nanosheets. Interestingly, ZnO for 10 wt% of zinc were nicely and evenly deposited on GO nanosheets as presented in Figs. 2(g) and (h). This is because the abundance of oxygen functional groups such as hydroxyl and epoxy in GO have provided active sites for reaction and attachment of ZnO, resulted in uniform distribution of ZnO on GO. Moreover, with lower concentration of Zn precursor, agglomeration of ZnO can be prevented. Obviously, the size of ZnO nanoparticles at 10 wt% of Zn was found to be smallest with uniform distribution.

It is worth noting that the ZnO nanoparticles have impregnated not only on the surface of the composites, but also on the inner layers of GO as shown in Fig. 3(a) for 10 wt% of Zn. The embedment of ZnO nanoparticles in the inner layers was able to prevent restacking of GO layers and maximize the composites surface area. In addition, the impregnation of ZnO in GO also prevented ZnO agglomeration problem as GO provided a matrix for heterogeneous growth of ZnO. Therefore, the overall surface area of the composites was enhanced. The size and distribution of ZnO on GO were further investigated by TEM as presented in Fig. 3(b). Similarly, the findings showed that the ZnO nanoparticles were distributed uniformly on GO nanosheets. The presence of Zn element in the composite was further confirmed by EDX mapping and spectra as shown in Figs. 3(c) and (d).

In next section, ZnO/rGO composite with 10 wt% of Zn was selected for membrane fabrication due to its highest

negative surface charge, smallest ZnO nanoparticle size and uniform distribution on GO nanosheets. The importance of these factors toward membrane fouling mitigation has been discussed in section 1.

3.2. Membranes characterization and performance testing

3.2.1. FTIR analysis of membranes

The interaction between PVDF and the inorganic fillers (ZnO and ZnO/rGO) could be observed via FTIR spectra as shown in Fig. 4. The typical peaks for PVDF could be seen clearly in all the membranes. The peaks at 1,406 and 1,079 cm^{-1} were associated with symmetrical stretching of CF_2 groups [29,30] while the peak of 1,188 cm^{-1} was caused by CF stretching vibration of CF_2 groups [9]. The peaks of 3,027 and 2,982 cm^{-1} were due to non-symmetrical and symmetrical stretching vibration of CH_2 groups [29]. Others typical peaks for PVDF such as 890, 847, 495 and 462 cm^{-1} were also found in all the membranes [31,32]. For ZnO MMMs, little changes could be identified on the spectra. However, no peaks were observed at 430 cm^{-1} due to Zn–O stretching mode and no absorption bands around 3,500 and 1,600 cm^{-1} (assigned to –OH groups of ZnO). Coincidently, this result was similar with previous studies done by Hong and He [9] and Zhang et al. [29] who also found weak interaction between ZnO and PVDF. On the other hand, FTIR spectra of ZnO/rGO MMMs showed good interaction of ZnO/rGO composite with PVDF. The absorption band of 3,300 cm^{-1} was assigned to –OH groups while 1,652 cm^{-1} was attributed to skeletal vibrations of unoxidized graphitic in ZnO/rGO composite [33]. The typical peaks of PVDF became sharper and shifted when blending with ZnO/rGO composite. For instance, the peak of 1,188 and 1,079 cm^{-1} have shifted to 1,180 and 1,067 cm^{-1}, respectively.

3.2.2. Membrane permeability and hydrophilicity

Membrane contact angle is the measurement of membranes' hydrophilicity. As presented in Fig. 5, the contact angle of pure PVDF membrane was 80.97°. The addition of ZnO nanoparticles and ZnO/rGO composite as inorganic fillers had reduced the membrane contact angle to 79.47° and 68.63°, respectively. The reduced contact angle implied that

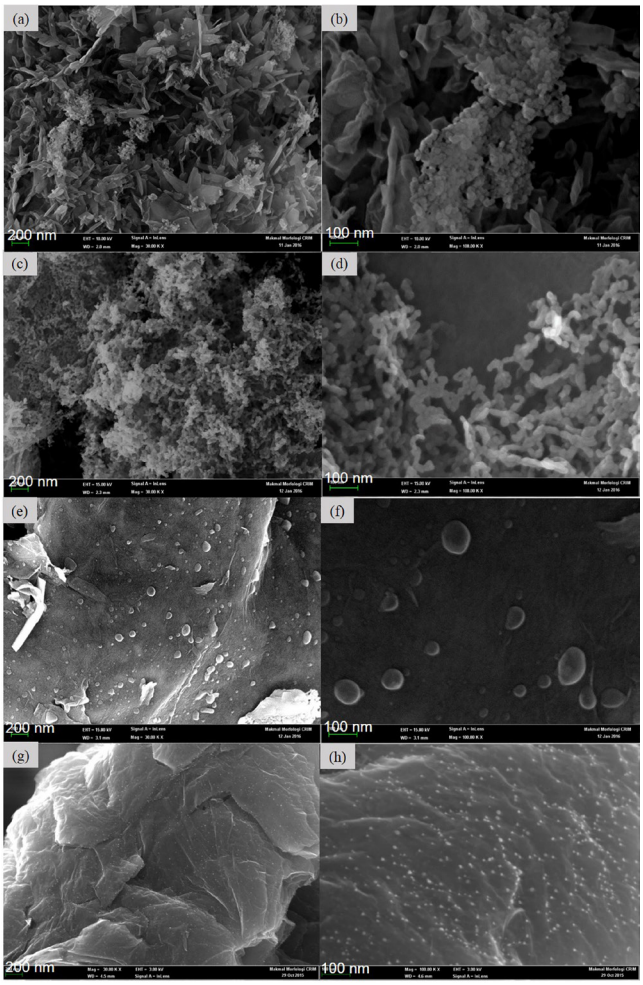

Fig. 2. Distribution of ZnO on GO nanosheets for (a) and (b) 100 wt%; (c) and (d) 60 wt% (e) and (f) 30 wt% and (g) and (h) 10 wt% of Zn at magnification of 30,000× and 100,000×.

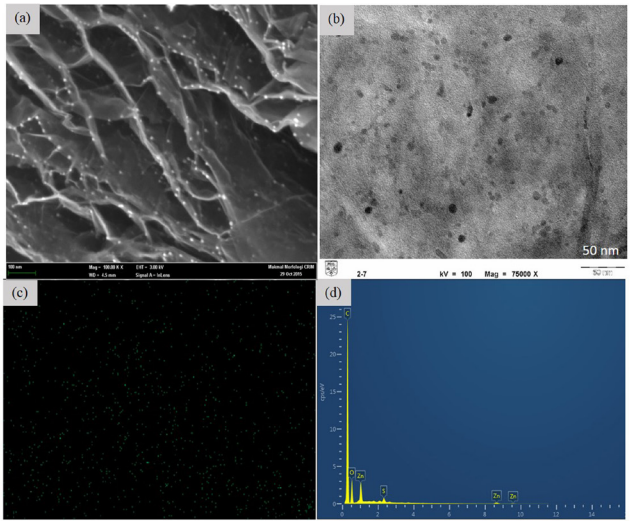

Fig. 3. (a) FESEM image of ZnO impregnated in GO at 100,000× magnification, (b) TEM image, (c) EDX mapping and (d) EDX spectra, of 10 wt% of Zn composite.

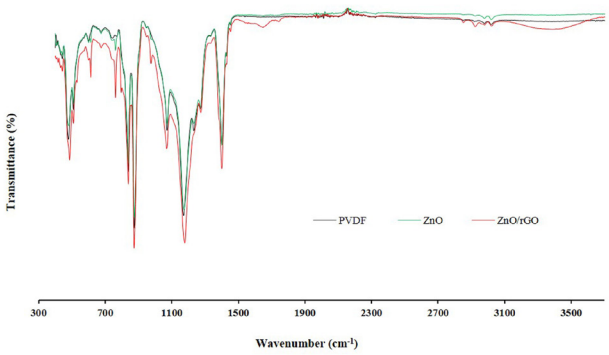

Fig. 4. FTIR spectra of neat PVDF membranes, ZnO MMMs and ZnO/rGO MMMs.

the oxygen functional groups of the inorganic fillers have attracted the water molecule toward the membrane, proving that the hydrophilicity effect was dominant in the formation of PVDF–ZnO MMMs and PVDF–ZnO/rGO MMMs [5,34]. Similarly to previous studies, the permeation flux of pure water obtained in this study was correlated with hydrophilicity improvement of the membranes. The pure water flux of ZnO MMMs and ZnO/rGO MMMs increased by 40% and 61%, respectively, compared with neat PVDF membranes. The increment of ZnO/rGO MMMs' permeability in this study was comparatively higher than others PVDF MMMs which incorporated with metal oxide such as TiO_2 [35,36], Ag [37] and SiO_2 [38]. Besides, the higher permeation flux of ZnO/rGO MMMs was also attributed to the formation of bigger pore size during phase inversion process. Based on the findings in Fig. 6, the neat membrane pore size increased from 25 to 28 nm and 31 nm, with the addition of ZnO nanoparticles and ZnO/rGO composites, respectively. As ZnO/rGO are highly hydrophilic, the addition of these composites had enhanced the mass transfer between the solvent (DMAc) and non-solvent (water) during the phase inversion process, resulting in bigger membrane pore size [39]. Meanwhile, the neat PVDF membranes porosity increased from 34% to 69% and 73% with the addition of ZnO and ZnO/rGO, respectively. The surface and inner

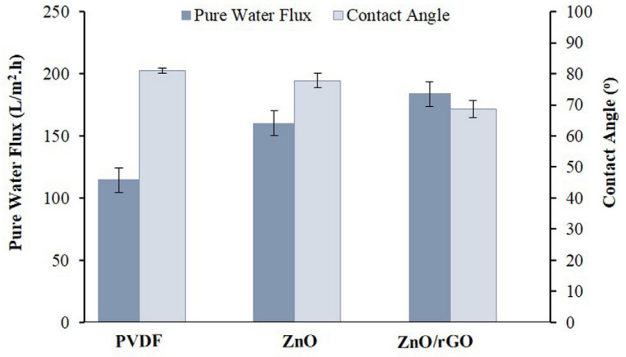

Fig. 5. Pure water flux and contact angle of neat PVDF membranes, ZnO MMMs and ZnO/rGO MMMs.

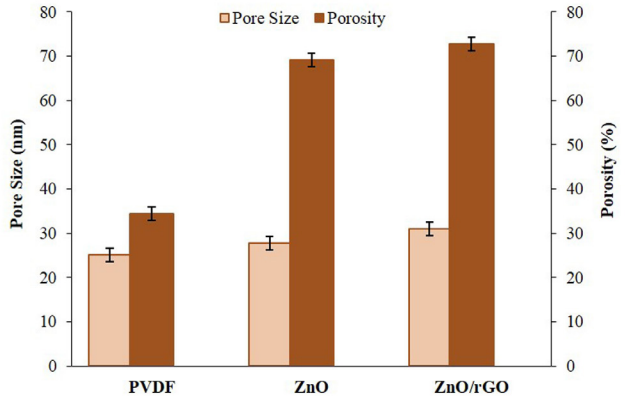

Fig. 6. Pore size and porosity of neat PVDF membranes, ZnO MMMs and ZnO/rGO MMMs.

structure of the membranes were observed via FESEM and would be further discussed.

3.2.3. Membrane morphology

Figs. 7(a)–(c) show the three-dimensional surface morphology of membranes at a scan size of 5 μm × 5 μm. The roughness parameters such as average roughness (S_a), root mean square roughness (S_q) and average height of five highest peaks and five lowest valleys (S_z) of the membranes are indicated in Fig. 7(d). The overall membrane surface roughness increased with addition of ZnO nanoparticles but decreased with incorporation of ZnO/rGO composites. The rougher membrane surface of ZnO MMMs may cause by agglomeration of ZnO nanoparticles in the polymer solution. According to Wenzel model, surface roughness would affect membrane's water wettability. Hydrophilic surface will become more hydrophilic when surface roughness increases [40]. This theory support the result where the contact angle dropped (section 3.2.2) when the surface roughness of PVDF membranes increased. Coincidently, this was similar with a study done by Jafarzadeh et al. [41] where incorporation of ZnO increased the membrane surface roughness. On the other hand, ZnO nanoparticles were distributed uniformly on GO nanosheets and therefore reduced agglomeration problem in the polymer solution. As a result, the height difference of peaks and valleys on ZnO/rGO MMMs surface was greatly reduced. As GO contains abundance amount of oxygen functional groups, the hydrophilicity of ZnO/rGO composites became dominant and resulted in contact angle decrement. Generally, smooth surface topography could prevent the deposition of foulant on membrane surface. Hence, the antifouling ability of ZnO/rGO MMMs improved tremendously when tested with BSA solution (section 3.3).

FESEM images of top surface and cross-sectional view of membranes are presented in Fig. 8. As shown in Figs. 8(a), (c) and (e), the pore size observed on neat PVDF membrane was tiny and could hardly be seen. Meanwhile, the pore size observed on ZnO and ZnO/rGO membrane surface were generally bigger and pore density were higher. For cross-sectional view, the neat PVDF membrane without any pore forming agent like PVP exhibited short finger-like structure with mainly sponge substrates. This indicated slower phase inversion happened during immersion-precipitation process due to the hydrophobic nature of PVDF polymer [42]. With addition of ZnO or ZnO/rGO into the PVDF polymer solution, the casting solutions became hydrophilic. The oxygen functional groups had introduced greater amount of non-solvent into the PVDF casting solutions, induced faster solvent and non-solvent interdiffusion velocity and therefore accelerated the phase inversion process. As a result, longer finger-like structures are observed in Figs. 8(d) and (f) for MMMs. In comparison, Fig. 8(f) (ZnO/rGO MMMs) gives the longest and biggest pore structure and eventually resulted in higher membrane porosity.

The distribution of ZnO/rGO composites throughout the membranes was identified by EDX mapping as shown in Fig. 9. The green dots shown in Figs. 9(a) and (c) are fluoride (F) element contained in PVDF polymer while the blue dots in Figs. 9(c) and (d) are Zn element of ZnO/rGO composite. The blue dots are distributed evenly in both of the plan and

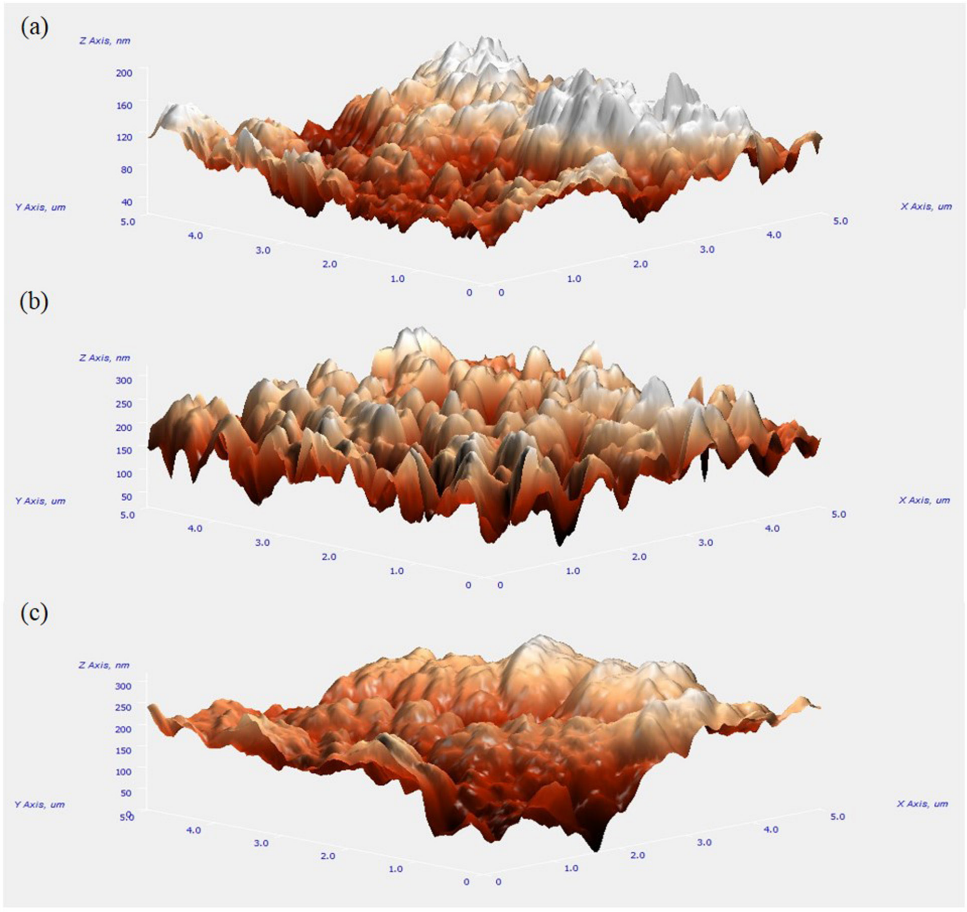

(d)

Membrane	S_a	S_q	S_z
Neat PVDF Membranes	31.00 ± 7.11	38.94 ± 8.68	253.28 ± 26.52
ZnO MMMs	51.47 ± 8.86	63.28 ± 10.75	371.66 ± 63.28
ZnO/rGO MMMs	27.49 ± 10.30	34.03 ± 12.01	189.68 ± 54.20

Sa: average roughness; Sq: root mean square roughness; Sx: average height of five highest peaks and five lowest valleys.

Fig. 7. AFM three-dimensional surface morphology of (a) neat PVDF membrane, (b) ZnO MMMs, (c) ZnO/rGO MMMs and (d) roughness parameters.

sectional view of membranes, indicating ZnO/rGO composites were well dispersed in the PVDF membranes.

3.3. Membrane filtration behavior

The antifouling property of membranes could be evaluated by filtration with BSA solution. As PVDF membranes were hydrophobic in nature, the initial and overall permeation flux of neat PVDF membranes were always within a lower range as illustrated in Fig. 10. The filtration rate declined steadily as foulant deposited on the membrane surface. In contrast, pore blockage by BSA occurred at the first 15 min in ZnO MMMs and ZnO/rGO MMMs with larger pore size, resulting in rapid drop of initial flux [28]. The subsequent gradual decline was attributed to deposition of foulant on the membranes surface. The average BSA filtration of neat PVDF membranes, ZnO MMMs and ZnO/rGO MMMs are 12, 47 and 64 L/m^2 h, respectively. As can be observed from the graph, the MMMs' flux always higher than neat PVDF membrane over the 210 min pure water and BSA filtration. Moreover, the BSA rejection of neat PVDF membranes, ZnO MMMs and ZnO/rGO MMMs are 15%, 24% and 32%, respectively. Therefore, it could be concluded that the PVDF membranes' rejection and antifouling property was successfully improved with addition of hydrophilic ZnO and ZnO/rGO. Obviously, ZnO/rGO MMMs with greatest hydrophilicity (lowest contact angle) gave the highest BSA rejection and permeation flux over the filtration process. The enhanced membrane hydrophilicity would be essential in the formation of water boundary layer on the membrane via hydrogen bond between the water molecules and oxygen

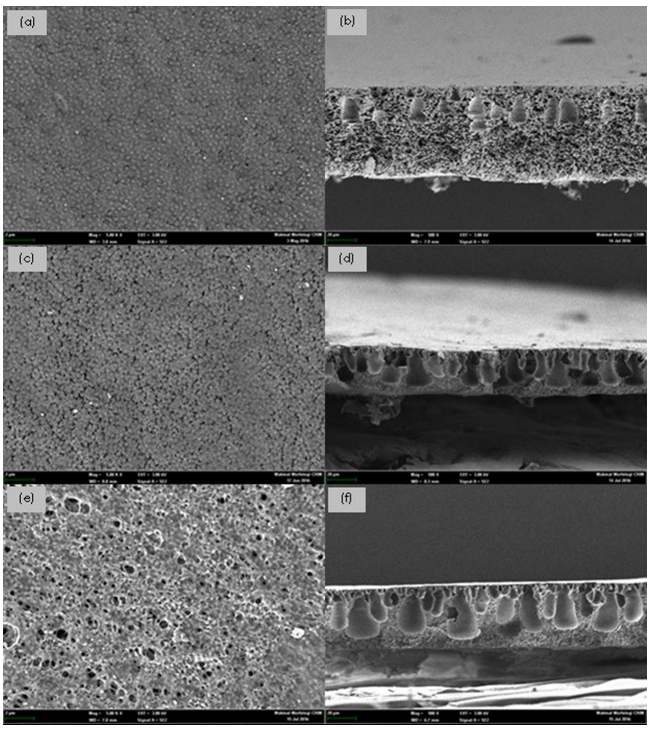

Fig. 8. FESEM images of surface (5,000× magnification) and cross-sectional (500× magnification) morphology of (a) and (b) neat PVDF membranes, (c) and (d) ZnO MMMs and (e) and (f) ZnO/rGO MMMs.

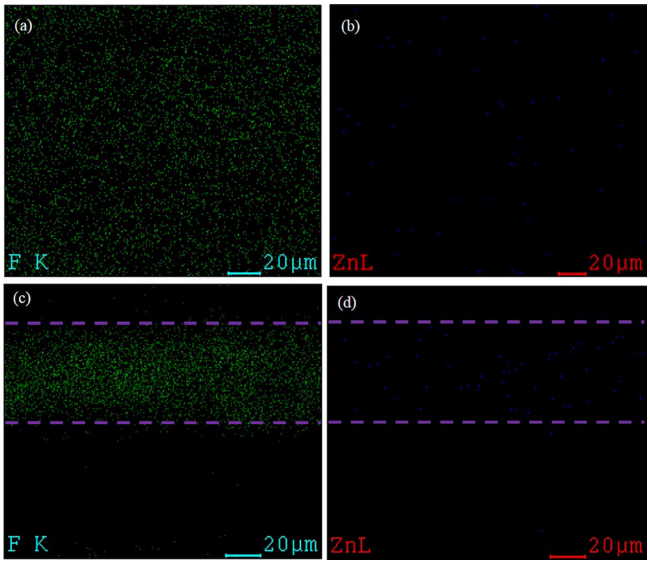

Fig. 9. Mapping images of F and Zn element on (a) and (b) top surface, and (c) and (d) sectional view of ZnO/rGO MMMs.

functional groups of the ZnO nanohybrids embedded in the membranes, preventing the contact and adsorption of foulant onto the membranes surface [20,43]. Besides, surface charge of ZnO/rGO composites also contributed to the membrane's antifouling ability. The surface charge of neat PVDF membranes, ZnO MMMs and ZnO/rGO MMMs was –18.9, +1.07

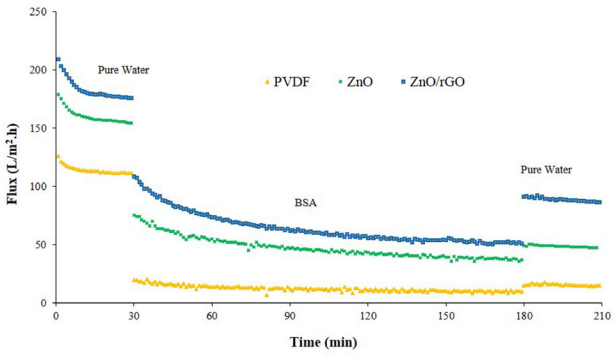

Fig. 10. Flux decline of neat PVDF membranes, ZnO MMMs and ZnO/rGO MMMs during BSA filtration.

and –29.7 mV, respectively. The high negative charge MMMs tended to repel with BSA which was negatively charge at neutral pH [44]. The antifouling property of the membranes could be further explained with FRR. The FRR of all the membranes were calculated and compared. In this study, the FRR value of neat PVDF, ZnO and ZnO/rGO membrane was 17%, 30% and 48%, respectively. Hence, this had proven that ZnO/rGO blended membranes exhibited the greatest antifouling ability as higher FRR value signified better antifouling property of the membranes.

3.4. Leaching analysis

Leaching test was performed to examine the reliability of the MMMs to use for long-term filtration. When the amount of fillers embedded in the MMMs reduced, the performance of membranes would drop accordingly. Besides, the leaching of metal oxide into the water would give negative impact to the environment especially aquatic life [45]. The stability of inorganic fillers in the MMMs was investigated by examining the release of Zn element in permeate during the 6 h filtration. The release of Zn element from ZnO MMMs was 7, 3 and 2 ppb for the first 3 h and no further leaching afterwards. On the other hand, no Zn element was detected in permeate of ZnO/rGO MMMs during the 6 h filtration. This finding could be supported by the result from FTIR in section 3.2.1 where the interaction between ZnO and PVDF was weak. Hence, the tendency of ZnO to leach from the membrane surface was higher. Similar leaching was observed by Li et al. [46] for PVDF MMMs embedded with in situ formation of Ag nanoparticles. Meanwhile, the presence of oxygen functional groups (hydroxyl, epoxide, carbonyl and carboxyl) in ZnO/rGO composites have formed strong interaction with PVDF molecular chains. The hydrogen bonds formed between C–F bond of PVDF and oxygen functional groups of ZnO/rGO composite had enhanced their interfacial interaction, therefore, no leaching of composites was detected in the permeate.

3.5. Antibacterial activity of membranes

The images in Fig. 11 show that ZnO and ZnO/rGO MMMs exhibited good antibacterial ability toward *E. coli*. The neat PVDF membranes did not show any bacteria resistance as its surface was covered by growth of dense *E. coli* (Fig. 11(a)).

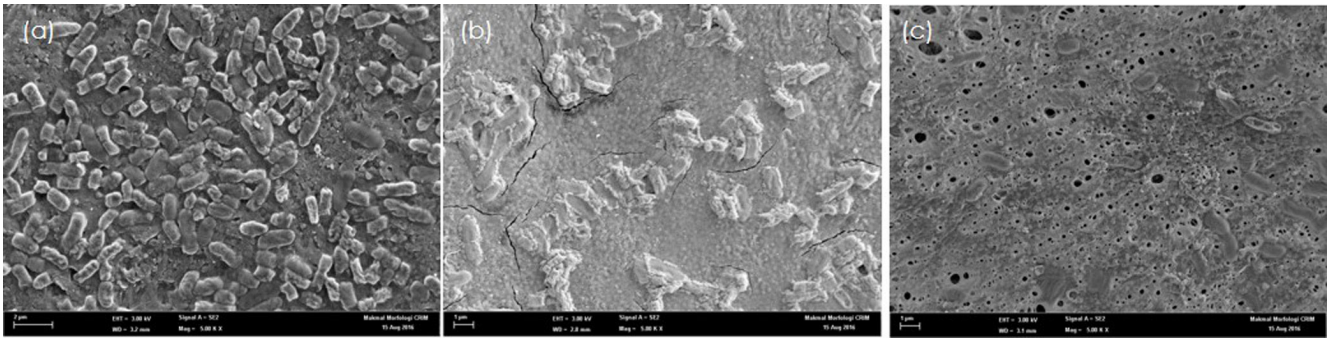

Fig. 11. FESEM images (5,000× magnification) of bacteria grew on surface of (a) neat PVDF membrane, (b) ZnO MMMs and (c) ZnO/rGO MMMs.

Typically, a dense layer of biofilm would form on PVDF membranes surface during filtration process due to the hydrophobic instinct of PVDF, promoted adherent of non-polar solute and bacteria [46]. On the other hand, only a few colonies of *E. coli* were observed on ZnO MMMs surface (Fig. 11(b)). Interestingly, ZnO/rGO MMMs showed impressive outcome with only a few *E. coli* were noticed on the membrane surface (Fig. 11(c)). The antibacterial activity test had proven that ZnO/rGO MMMs possessed excellent antibacterial effect against *E. coli*. The rapid electron transfer between ZnO and GO in the composite and adsorption of surface oxygen by GO have resulted in formation of higher amount of ROS which were dominant in destroying bacteria cell membranes [47]. However, the antibacterial mechanism of ZnO under dark condition is currently under a huge debate. Prasanna and Vijayaraghavan [48] found that ROS was significantly produced from ZnO even in dark condition; therefore, ROS was proposed as the dominant mechanism. However, a recent study done by Joe et al. [49] revealed that bacterial cells were mainly being destroyed by local dissolution of ZnO, releasing Zn^{2+} ions into the bacterial cytoplasm. Therefore, more studies should be performed on the investigation of antibacterial mechanism of ZnO/rGO composites under dark condition.

4. Conclusion

Properties of PVDF membrane as one of the most widely used membranes in the industry was enhanced by blending with ZnO nanoparticles and ZnO/rGO composites. ZnO/rGO composites gave the highest hydrophilic effect to the PVDF membranes. Hence, the permeation flux was increased due to the formation of bigger finger-like microvoids during phase inversion process. The higher BSA rejection and FRR of ZnO/rGO MMMs proved that the rejection and antifouling ability of the modified membranes was enhanced. There was no Zn element detected in permeate of ZnO/rGO MMMs, implied the strong interaction between ZnO/rGO composites and PVDF membranes. Therefore, the ZnO/rGO MMMs exhibited high potential in industrial membrane applications. In addition, the excellent antibacterial property of ZnO/rGO MMMs showed great potential in controlling membrane biofouling, hence it is highly recommended to be utilized in biological treated wastewater filtration process. In brief, the incorporation of ZnO/rGO composites in PVDF membranes had exhibited high potential in various industrial applications due to its enhancement in terms of hydrophilicity, permeability, antifouling ability and antibacterial property.

Acknowledgments

This study was financially supported by Universiti Kebangsaan Malaysia (Grant No. ICONIC-2013-002). Besides, the authors wish to acknowledge CEGT (Center for Environment and Green Technology, UTAR, IPSR/RMC/UTARRF/2016-C1/P1) and CRIM (Center for Research and Instrumentation Management, UKM) for their supports in this work.

References

[1] F.I. Hai, K. Yamamoto, C.-H. Lee, Membrane Biological Reactors – Theory, Modeling, Design, Management and Applications to Wastewater Reuse, IWA Publishing, London, 2014.
[2] S. Judd, The MBR Book: Principles and Applications of Membrane Bioreactors for Water and Wastewater Treatment, Elsevier, Oxford, 2010.
[3] H.L. Richards, P.G.L. Baker, E. Iwuoha, Metal nanoparticle modified polysulfone membranes for use in wastewater treatment: a critical review, J. Surf. Eng. Mater. Adv. Technol., 2 (2012) 183–193.
[4] L.Y. Ng, A.W. Mohammad, C.P. Leo, N. Hilal, Polymeric membranes incorporated with metal/metal oxide nanoparticles: a comprehensive review, Desalination, 308 (2013) 15–33.
[5] E. Yuliwati, A.F. Ismail, Effect of additives concentration on the surface properties and performance of PVDF ultrafiltration membranes for refinery produced wastewater treatment, Desalination, 273 (2011) 226–234.
[6] M. Kumar, Z. Gholamvand, A. Morrissey, K. Nolan, M. Ulbricht, J. Lawler, Preparation and characterization of low fouling novel hybrid ultrafiltration membranes based on the blends of GO–TiO_2 nanocomposite and polysulfone for humic acid removal, J. Membr. Sci., 506 (2016) 38–49.
[7] E. Mahmoudi, L.Y. Ng, M.M. Ba-Abbad, A.W. Mohammad, Novel nanohybrid polysulfone membrane embedded with silver nanoparticles on graphene oxide nanoplates, Chem. Eng. J., 277 (2015) 1–10.
[8] L. Huang, S. Zhao, Z. Wang, J. Wu, J. Wang, S. Wang, In situ immobilization of silver nanoparticles for improving permeability, antifouling and anti-bacterial properties of ultrafiltration membrane, J. Membr. Sci., 499 (2016) 269–281.
[9] J. Hong, Y. He, Polyvinylidene fluoride ultrafiltration membrane blended with nano-ZnO particle for photo-catalysis self-cleaning, Desalination, 332 (2014) 67–75.
[10] S. Liang, K. Xiao, Y. Mo, X. Huang, A novel ZnO nanoparticle blended polyvinylidene fluoride membrane for anti-irreversible fouling, J. Membr. Sci., 394–395 (2012) 184–192.

[11] M.R. Mehrnia, Y.M. Mojtahedi, M. Homayoonfal, What is the concentration threshold of nanoparticles within the membrane structure? A case study of Al_2O_3/Psf nanocomposite membrane, Desalination, 372 (2015) 75–88.
[12] K.R. Raghupathi, R.T. Koodali, A.C. Manna, Size-dependent bacterial growth inhibition and mechanism of antibacterial activity of zinc oxide nanoparticles, Langmuir, 27 (2011) 4020–4028.
[13] Y.T. Chung, M.M. Ba-Abbad, A.W. Mohammad, A. Benamor, Functionalization of zinc oxide (ZnO) nanoparticles and its effects on polysulfone-ZnO membranes, Desal. Wat. Treat., 57 (2016) 7801–7811.
[14] J. Hong, Y. He, Effects of nano sized zinc oxide on the performance of PVDF microfiltration membranes, Desalination, 302 (2012) 71–79.
[15] C.P. Leo, W.P. Cathie Lee, A.L. Ahmad, A.W. Mohammad, Polysulfone membranes blended with ZnO nanoparticles for reducing fouling by oleic acid, Sep. Purif. Technol., 89 (2012) 51–56.
[16] R. Marsalek, Particle size and zeta potential of ZnO, APCBEE Procedia, 9 (2014) 13–17.
[17] D. Ramimoghadam, M.Z. Bin Hussein, Y.H. Taufiq-Yap, The effect of sodium dodecyl sulfate (SDS) and cetyltrimethylammonium bromide (CTAB) on the properties of ZnO synthesized by hydrothermal method, Int. J. Mol. Sci., 13 (2012) 13275–13293.
[18] N.H.H. Hairom, A.W. Mohammad, A.A.H. Kadhum, Influence of zinc oxide nanoparticles in the nanofiltration of hazardous Congo red dyes, Chem. Eng. J., 260 (2015) 907–915.
[19] F.S. Omar, H.N. Ming, S.M. Hafiz, L.H. Ngee, Microwave synthesis of zinc oxide/reduced graphene oxide hybrid for adsorption-photocatalysis application, Int. J. Photoenergy, 2014 (2014) 1–9.
[20] J. Lee, H.-R. Chae, Y.J. Won, K. Lee, C.-H. Lee, H.H. Lee, I.-C. Kim, J. Lee, Graphene oxide nanoplatelets composite membrane with hydrophilic and antifouling properties for wastewater treatment, J. Membr. Sci., 448 (2013) 223–230.
[21] S. Zinadini, V. Vatanpour, A.A. Zinatizadeh, M. Rahimi, Z. Rahimi, M. Kian, Preparation and characterization of antifouling graphene oxide/polyethersulfone ultrafiltration membrane: application in MBR for dairy wastewater treatment, J. Water Process Eng., 7 (2015) 280–294.
[22] T. Gordon, B. Perlstein, O. Houbara, I. Felner, E. Banin, S. Margel, Synthesis and characterization of zinc/iron oxide composite nanoparticles and their antibacterial properties, Colloids Surf., A, 374 (2011) 1–8.
[23] R. Sonohara, N. Muramatsu, H. Ohshima, T. Kondo, Difference in surface properties between *Escherichia coli* and *Staphylococcus aureus* as revealed by electrophoretic mobility measurements, Biophys. Chem., 55 (1995) 273–277.
[24] S.Y. Xie, X. Bin Li, Y.Y. Sun, Y.L. Zhang, D. Han, W.Q. Tian, W.Q. Wang, Y.S. Zheng, S.B. Zhang, H.B. Sun, Theoretical characterization of reduction dynamics for graphene oxide by alkaline-earth metals, Carbon, 52 (2013) 122–127.
[25] X. Zhao, J.Y. Lee, C.-R. Kim, J. Heo, C.M. Shin, J.-Y. Leem, H. Ryu, J.-H. Chang, H.C. Lee, W.-G. Jung, Dependence of the properties of hydrothermally grown ZnO on precursor concentration, Physica E Low-Dimens. Syst. Nanostruct., 41 (2009) 1423–1426.
[26] M.F. Malek, M.H. Mamat, M.Z. Sahdan, M.M. Zahidi, Z. Khusaimi, M.R. Mahmood, Influence of various sol concentrations on stress/strain and properties of ZnO thin films synthesised by sol–gel technique, Thin Solid Films, 527 (2013) 102–109.
[27] A.G. Vega-Poot, G. Rodriguez-Gattorno, O.E. Soberanis-Dominguez, R.T. Patino-Diaz, M. Espinosa-Pesqueira, G. Oskam, The nucleation kinetics of ZnO nanoparticles from $ZnCl_2$ in ethanol solutions, Nanoscale, 2 (2010) 2710–2717.
[28] S. Xia, M. Ni, Preparation of poly(vinylidene fluoride) membranes with graphene oxide addition for natural organic matter removal, J. Membr. Sci., 473 (2014) 54–62.
[29] X. Zhang, Y. Wang, Y. Liu, J. Xu, Y. Han, X. Xu, Preparation, performances of PVDF/ZnO hybrid membranes and their applications in the removal of copper ions, Appl. Surf. Sci., 316 (2014) 333–340.
[30] F.A. Sheikh, M.A. Zargar, A.H. Tamboli, H. Kim, A super hydrophilic modification of poly(vinylidene fluoride) (PVDF) nanofibers: by in situ hydrothermal approach, Appl. Surf. Sci., 385 (2016) 417–425.
[31] E. Freire, O. Bianchi, J.N. Martins, E.E.C. Monteiro, M.M.C. Forte, Non-isothermal crystallization of PVDF/PMMA blends processed in low and high shear mixers, J. Non-Cryst. Solids, 358 (2012) 2674–2681.
[32] N. Ataollahi, A. Ahmad, H. Hamzah, M.Y.A. Rahman, N.S. Mohamed, Preparation and characterization of PVDF-HFP/MG49 based polymer blend electrolyte, Int. J. Electrochem. Sci., 7 (2012) 6693–6703.
[33] Y. Wang, J. Liu, L. Liu, D.D. Sun, High-quality reduced graphene oxide-nanocrystalline platinum hybrid materials prepared by simultaneous co-reduction of graphene oxide and chloroplatinic acid, Nanoscale Res. Lett., 6 (2011) 1–8.
[34] S. Zhao, W. Yan, M. Shi, Z. Wang, J. Wang, S. Wang, Improving permeability and antifouling performance of polyethersulfone ultrafiltration membrane by incorporation of ZnO-DMF dispersion containing nano-ZnO and polyvinylpyrrolidone, J. Membr. Sci., 478 (2015) 105–116.
[35] B.S. Kim, J. Lee, Macroporous PVDF/TiO_2 membranes with three-dimensionally interconnected pore structures produced by directional melt crystallization, Chem. Eng. J., 301 (2016) 158–165.
[36] W. Hu, J. Yin, B. Deng, Z. Hu, Application of nano TiO_2 modified hollow fiber membranes in algal membrane bioreactors for high-density algae cultivation and wastewater polishing, Bioresour. Technol., 193 (2015) 135–141.
[37] H. Shi, F. Liu, L. Xue, H. Lu, Q. Zhou, Enhancing antibacterial performances of PVDF hollow fibers by embedding Ag-loaded zeolites on the membrane outer layer via co-extruding technique, Compos. Sci. Technol., 96 (2014) 1–6.
[38] H.P. Ngang, A.L. Ahmad, S.C. Low, B.S. Ooi, Preparation of thermoresponsive PVDF/SiO_2-PNIPAM mixed matrix membrane for saline oil emulsion separation and its cleaning efficiency, Desalination, 408 (2017) 1–12.
[39] M. Mulder, Basic Principles of Membrane Technology, Kluwer Academic Publishers, Enschede, 1996.
[40] R.N. Wenzel, Resistance of solid surfaces to wetting by water, J. Ind. Eng. Chem., 28 (1936) 988–994.
[41] Y. Jafarzadeh, R. Yegani, M. Sedaghat, Preparation, characterization and fouling analysis of ZnO/polyethylene hybrid membranes for collagen separation, Chem. Eng. Res. Des., 94 (2015) 417–427.
[42] M.L. Yeow, Y.T. Liu, K. Li, Morphological study of poly(vinylidene fluoride) asymmetric membranes: effects of the solvent, additive, and dope temperature, J. Appl. Polym. Sci., 92 (2004) 1782–1789.
[43] G. Kang, Y. Cao, Application and modification of poly(vinylidene fluoride) (PVDF) membranes – a review, J. Membr. Sci., 463 (2014) 145–165.
[44] Z.X. Low, A. Razmjou, K. Wang, S. Gray, M. Duke, H. Wang, Effect of addition of two-dimensional ZIF-L nanoflakes on the properties of polyethersulfone ultrafiltration membrane, J. Membr. Sci., 460 (2014) 9–17.
[45] E. Casals, E. González, V. Puntes, Inorganic Nanoparticles and the Environment: Balancing Benefits and Risks, M. Farré, D. Barceló, Eds., Comprehensive Analytical Chemistry, Vol. 59, 2012, pp. 265–290.
[46] X. Li, R. Pang, J. Li, X. Sun, J. Shen, W. Han, L. Wang, In situ formation of Ag nanoparticles in PVDF ultrafiltration membrane to mitigate organic and bacterial fouling, Desalination, 324 (2013) 48–56.
[47] L. Zhong, K. Yun, Graphene oxide-modified ZnO particles: synthesis, characterization, and antibacterial properties, Int. J. Nanomed., 10 (2015) 79–92.
[48] V.L. Prasanna, R. Vijayaraghavan, Insight into the mechanism of antibacterial activity of ZnO – surface defects mediated reactive oxygen species even in dark, Langmuir, 31 (2015) 1–29.
[49] A. Joe, S. Park, K. Shim, D. Kim, K. Jhee, H. Lee, C. Heo, H. Kim, E. Jang, Antibacterial mechanism of ZnO nanoparticles under dark conditions, J. Ind. Eng. Chem., 45 (2017) 430–439.